



ELSEVIER

Available online at www.sciencedirect.com

ScienceDirect

journal homepage: www.elsevier.com/locate/he

Synthesis and thermal decomposition of potassium tetraamidoboranealuminate, $K[Al(NH_2BH_3)_4]$

Kasper T. Møller^a, Mathias Jørgensen^a, Jacob G. Andreasen^a,
Jørgen Skibsted^a, Zbigniew Łodziana^b, Yaroslav Filinchuk^c,
Torben R. Jensen^{a,*}

^a Interdisciplinary Nanoscience Center (iNANO) and Department of Chemistry, University of Aarhus, DK-8000 Aarhus, Denmark

^b Department of Structural Research, INP Polish Academy of Sciences, ul. Radzikowskiego 152, 31-342 Krakow, Poland

^c Institute of Condensed Matter and Nanosciences, Université Catholique de Louvain, Place L. Pasteur 1, 1348 Louvain-la-Neuve, Belgium

ARTICLE INFO

Article history:

Received 25 August 2017

Received in revised form

9 November 2017

Accepted 10 November 2017

Available online 6 December 2017

Keywords:

Hydrogen storage

Metal amidoboranes

Potassium alanate

Ammonia borane

Potassium

tetraamidoboranealuminate

ABSTRACT

A new potassium tetraamidoboranealuminate, $K[Al(NH_2BH_3)_4]$, has been synthesized by a mechanochemical reaction between $KAlH_4$ and NH_3BH_3 . The compound, $K[Al(NH_2BH_3)_4]$, crystallizes in a triclinic unit cell with space group symmetry $P\bar{1}$. The crystal structure consists of $[K(NH_2BH_3)_6]^{5-}$ octahedra which facilitate the bridging between K^+ in 1D chains, while also bridging K^+ to Al^{3+} to connect the 1D chains in a 3D network. Thermal analysis reveals that $K[Al(NH_2BH_3)_4]$ decomposes in two exothermic steps at $T \sim 94$ and 138 °C and releases primarily hydrogen. The total gas release amounts to ~ 6.0 wt% H_2 . The decomposition products are investigated *ex situ* by powder X-ray diffraction, infrared spectroscopy, and ^{11}B and ^{27}Al NMR and identified as KBH_4 and amorphous phases, possibly BN_3 , N_2BH , and/or NBH_2 whereas aluminum is found in four-, five-, and six-fold coordination. Unfortunately, the decomposed sample shows no hydrogen absorption at $T = 260$ °C and $p(H_2) = 110$ bar.

© 2017 Hydrogen Energy Publications LLC. Published by Elsevier Ltd. All rights reserved.

Introduction

Hydrogen has a great potential as an energy carrier [1–6]. Thus, research within hydrogen storage materials has primarily focused on the discovery of possible successors for liquid fuels, diesel and gasoline, appropriate for mobile

applications [7–11]. Initially, aluminum-based hydrides attracted significant attention as the reversible system $NaAlH_4-TiCl_3$ was discovered [12]. However, $KAlH_4$ has the advantage over $NaAlH_4$ that no additives are needed to promote the reversible hydrogen release and uptake at low pressures (<10 bar) and moderate temperatures (250–300 °C) [13]. Yet, the detailed decomposition mechanism of $KAlH_4$ is

* Corresponding author. Center for Materials Crystallography, iNANO and Department of Chemistry, Langelandsgade 140, D-8000 Aarhus C, Aarhus University, Denmark.

E-mail address: trj@chem.au.dk (T.R. Jensen).

<https://doi.org/10.1016/j.ijhydene.2017.11.080>

0360-3199/© 2017 Hydrogen Energy Publications LLC. Published by Elsevier Ltd. All rights reserved.

still debated and the possible intermediates remain not fully characterized [14,15]. Additionally, the reversibility conditions for KAlH_4 are too harsh for mobile applications, hence optimization of KAlH_4 is required if utilization is to be realized.

Nitrogen-boron containing compounds have also been extensively studied [16–19]. A compound which has received great attention is ammonia borane, NH_3BH_3 , owing to its high gravimetric hydrogen density, $\rho_m = 19.6$ wt% H_2 [20–23]. However, for mobile applications, NH_3BH_3 has several drawbacks. The decomposition occurs in two steps below 200 °C, with release of toxic gasses, e.g. ammonia (NH_3), diborane (B_2H_6) and borazine ($\text{N}_3\text{B}_3\text{H}_3$) whilst the first decomposition step is exothermic ($\Delta H_{\text{dec}} = -21.7$ kJ/mol H_2) and hence irreversible [20,24–26]. Many attempts have been made to improve these properties, especially through metal amidoboranes, which often have high gravimetric hydrogen densities, fast kinetics, and low decomposition temperatures, whereas the purity of hydrogen released is improved [16,27–32]. Moreover, metal borohydride–ammonia borane complexes, $\text{M}(\text{BH}_4)_x(\text{NH}_3\text{BH}_3)_y$ ($\text{M} = \text{Li}, \text{Mg}, \text{Ca}$), have been reported, however, they maintain the drawbacks of molecular NH_3BH_3 [33–36]. Finally, complexes combining aluminum, boron, and nitrogen have received increasing interest [37]. Especially, the combination of an aluminum atom bonded to multiple NH_3BH_3 residues may enable reversibility by combining the efficiency of NH_3BH_3 dehydrogenation with an aluminum-mediated hydrogenation process [38,39].

Recently, the first aluminum-based amidoborane, $\text{Na}[\text{Al}(\text{NH}_2\text{BH}_3)_4]$, was reported and found to decompose in two steps at 120 and 160 °C into NaBH_4 and amorphous products [40,41]. Interestingly, a partial reversibility of 1.7 mol H_2 was found between the two amorphous decomposition states [40]. Additionally, a few potassium-containing amidoboranes have been reported, e.g. KNH_2BH_3 and $\text{KNH}(\text{tBu})\text{BH}_3$ [28,30]. KNH_2BH_3 melts before an exothermic decomposition occurs at 80 °C and continues in two steps below 225 °C into an amorphous product which according to solid-state ^{11}B MAS NMR contains a branched polyiminoborane [30,42].

In this work, $\text{K}[\text{Al}(\text{NH}_2\text{BH}_3)_4]$ has been synthesized by mechanochemical treatment of KAlH_4 and NH_3BH_3 . The new potassium-based amidoborane compound has been characterized by *in-situ* synchrotron radiation powder X-ray diffraction (SR-PXD), density functional theory (DFT), thermogravimetric analysis combined with differential scanning calorimetry and simultaneous mass spectrometry (TG-DSC-MS), temperature programmed photographic analysis (TPPA), Sieverts' method (PCT), and solid-state ^{11}B and ^{27}Al magic-angle spinning (MAS) NMR.

Experimental

Sample preparation

KH (Sigma–Aldrich, 30 wt% dispersed in mineral oil) was initially dried under vacuum and washed three times with diethyl ether. Subsequently, Al (Strem Chemicals, 99.7%) and KH in a 1:1 molar ratio were loaded into a 80 mL tungsten carbide (WC) vial with WC balls (o.d. 10 mm) in a ball-to-powder mass ratio of 30:1 and ball milled for 48 cycles

consisting of 10 min milling and a 2 min break, giving a total of 8 h milling, using a Fritsch Pulverisette 6 planetary mill.

Finally, the ball-milled mixture was hydrogenated at $p(\text{H}_2) = 120$ bar and $T = 270$ °C for 12 h providing the product potassium alanate, KAlH_4 . KAlH_4 was then mixed with ammonia borane, NH_3BH_3 (Sigma–Aldrich, 97%), in the molar ratio 1:4 and ball milled in cycles consisting of 5 min milling and 2 min break with a ball-to-powder mass ratio of 30:1. Three samples were made using 96, 120, and 144 cycles giving a total milling time of 8, 10, and 12 h, respectively. The samples are denoted S1, S2, and S3, respectively.

Synchrotron radiation powder X-ray diffraction

High resolution, *in-situ* time-resolved SR-PXD data, used for crystal structure solution and refinement, were collected at beamline I11 at the Diamond Light source, Oxford, UK on a wide-angle position sensitive detector (PSD) based on Mythen-2 Si strip modules, $\lambda = 0.8259$ Å. The powdered sample was packed in quartz capillaries (i.d. 0.5 mm, wall thickness 0.01 mm) in an argon-filled glovebox ($p(\text{O}_2, \text{H}_2\text{O}) < 1$ ppm). Subsequently, the sample was heated from RT to 500 °C ($\Delta T/\Delta t = 5$ °C min^{-1}), while rotated during data acquisition. The temperature was calibrated using a NaCl standard [43]. The *in-situ* SR-PXD data plot has been background subtracted to clearly show the Bragg reflections.

Structure solution and refinement

The *in-situ* SR-PXD data (sample S3) were indexed using the DICVOL routine implemented in the software FOX [44], which revealed a triclinic unit cell. Subsequently, the structure was solved by global optimization in direct space, also using FOX. Structural models were created with one potassium atom, one aluminum atom, and four $[\text{NH}_2\text{BH}_3]^-$ groups treated as rigid bodies with N–B, N–H, and B–H distances of 1.589, 1.029, and 1.226 Å, respectively, and a number of antibump restraints to assist the convergence. The structure of $\text{K}[\text{Al}(\text{NH}_2\text{BH}_3)_4]$ was solved in space group P-1 and the structural model was refined using the Rietveld approach implemented in the software Fullprof [45].

Density functional theory

The initial, Rietveld-refined structure of $\text{K}[\text{Al}(\text{NH}_2\text{BH}_3)_4]$ was optimized with the conjugated gradient (CG) method with respect to the internal atomic positions. This procedure provided equilibrium hydrogen sites. As the second step, the unit cell shape was optimized. These optimized structures were subject to simulated annealing. No constraints were imposed on the internal atomic positions and the unit cell parameters were kept fixed for this procedure. The symmetry of the final structures was analyzed, and systems with imposed symmetry were re-optimized with the CG method. The electronic configurations of for H ($1s^1$), B ($2s^2 2p^1$), N ($2s^2 2p^3$), K ($3p^6 4s^1$), and Al ($3s^2 3p^1$) were represented by projected augmented wave potentials [46]. The gradient-corrected (GGA) functional and the corrections for a weak dispersive interaction were applied [47,48]. The plane wave formulation of the DFT method implemented in Vienna Simulation Package (VASP) was used [49].

The NMR parameters were calculated within the gauge-including projector augmented waves (GIPAW) approach [50,51]. PAW pseudopotentials were used and the geometry of the system was fixed. The isotropic shielding of BPO_4 at -3.60 ppm was used as the reference for ^{11}B [52], and for ^{27}Al : 16.0 ppm of $\alpha\text{-Al}_2\text{O}_3$ [53]. The quadrupolar coupling constant (C_Q) and the asymmetry parameter (η_Q) have been determined from the traceless electric field gradient (EFG), further details can be found elsewhere [54]. The nuclear quadrupole moments of 40.59 mb and 146.6 mb were used for the ^{11}B and ^{27}Al , respectively.

Thermal analysis

Thermogravimetric analysis and differential scanning calorimetry (TGA-DSC) of KAlH_4 and $\text{KAlH}_4\text{-NH}_3\text{BH}_3$ (1:4, **S3**) were performed on a PerkinElmer STA 6000 apparatus. The samples (approx. 4 mg) were placed in Al_2O_3 crucibles under protective argon atmosphere in a glovebox and heated from 40 to 300 °C ($\Delta T/\Delta t = 5$ °C min^{-1}) in an argon flow of 40 mL min^{-1} . Additionally, mass spectrometry data were simultaneously collected for H_2 , B_2H_6 , $\text{B}_3\text{H}_6\text{N}_3$ ($m/z = 80$), and NH_3 using a Hiden Analytical HPR-20 QMS sampling system.

Sieverts' measurement

The $\text{KAlH}_4\text{-NH}_3\text{BH}_3$ (1:4, **S3**) sample was transferred to a stainless steel high-temperature autoclave and connected to a custom-made Sieverts' apparatus [55]. Decomposition of the sample was performed by heating to $T = 200$ °C ($\Delta T/\Delta t = 3$ °C min^{-1}) for 1 h. Finally, the sample was cooled naturally to RT. Absorption was performed by heating the sample to $T = 260$ °C ($\Delta T/\Delta t = 5$ °C min^{-1}) at $p(\text{H}_2) = 110$ bar for 15 h. Subsequently, the sample was decomposed as described above.

Solid-state ^{11}B and ^{27}Al MAS NMR spectroscopy

The solid-state ^{11}B and ^{27}Al MAS NMR spectra were obtained on a Varian Direct-Drive VNMRs-600 spectrometer (14.1 T) using a custom-made CP/MAS NMR probe for 4 mm outer diameter rotors. The spectra employed a 0.5 μs excitation pulse for rf field strengths of $\gamma\text{B}_1/2\pi = 58$ kHz (^{11}B) or $\gamma\text{B}_1/2\pi = 70$ kHz (^{27}Al), relaxation delays of 4 s, 30 s (^{11}B) or 4 s (^{27}Al) and ^1H decoupling (TPPM, $\gamma\text{B}_2/2\pi = 42$ kHz). The experiments were performed at ambient temperature using airtight end-capped zirconia rotors packed with the samples in an argon-filled glovebox. Isotropic ^{11}B and ^{27}Al chemical shifts are relative to neat $\text{F}_3\text{B}\cdot\text{O}(\text{CH}_2\text{CH}_3)$ and an aqueous 1.0 M $\text{AlCl}_3\cdot 6\text{H}_2\text{O}$ solution, respectively. Simulations and least-squares optimizations to the manifold of spinning sidebands, observed for the ^{11}B and ^{27}Al satellite transitions, were performed using the STARS simulation software [56].

Fourier-transformed infrared spectroscopy

The sample $\text{KAlH}_4\text{-NH}_3\text{BH}_3$ (1:4, **S3**) was characterized by infrared absorption spectroscopy using a NICOLET 380 FT-IR instrument from Thermo Electron Corporation. The sample

was briefly exposed to air (~ 10 s) during transfer to the instrument.

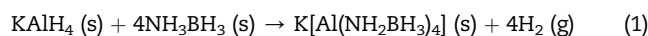
Temperature-programmed photographic analysis

Two pellets of **S1** and **S3** (~ 10 mg) were pressed and sealed under argon in a glass tube and placed in a custom-made aluminum heating block [57]. The samples were heated from RT to 200 °C ($\Delta T/\Delta t = 5$ °C min^{-1}) while photos of the sample were collected every six seconds.

Results

Initial sample analysis

Mechanochemical treatment of the reactants, $\text{KAlH}_4\text{-NH}_3\text{BH}_3$ (1:4), results in the appearance of a new set of Bragg reflections in the PXD pattern for all three samples, which was indexed in a triclinic unit cell: $a = 9.7151(3)$ Å, $b = 7.8221(3)$ Å, $c = 7.8750(3)$ Å, $\alpha = 95.358(3)^\circ$, $\beta = 109.944(3)^\circ$, and $\gamma = 89.629(3)^\circ$, $V = 559.74(4)$ Å³, and $Z = 2$. This diffraction data originates from a new compound, $\text{K}[\text{Al}(\text{NH}_2\text{BH}_3)_4]$, formed by the chemical reaction (1):



Rietveld refinement of the diffraction data of **S1** reveals a sample composition of $\text{K}[\text{Al}(\text{NH}_2\text{BH}_3)_4]$ (~ 67 wt%), KAlH_4 (~ 12 wt%), and NH_3BH_3 (~ 21 wt%). To enhance the formation of the new $\text{K}[\text{Al}(\text{NH}_2\text{BH}_3)_4]$ compound the ball-milling time was extended. Sample **S2** contains a major fraction of $\text{K}[\text{Al}(\text{NH}_2\text{BH}_3)_4]$ (~ 91 wt%) whereas only minor fractions of the reactants, KAlH_4 (~ 1.7 wt%) and NH_3BH_3 (~ 0.10 wt%) are present. However, Bragg reflections belonging to KBH_4 are now appearing and the amount was determined to be ~ 7.5 wt%. Longer ball-milling time, **S3**, results in additional formation of KBH_4 (~ 26 wt%), thus the $\text{K}[\text{Al}(\text{NH}_2\text{BH}_3)_4]$ decomposes under extensive ball milling (see later section on decomposition products). Furthermore, **S3** contains $\text{K}[\text{Al}(\text{NH}_2\text{BH}_3)_4]$ (~ 67 wt%), NH_3BH_3 (~ 3.6 wt%), and KAlH_4 (~ 3.1 wt%), see also Table 1 for an overview of the approximate sample composition. However, the structural solution was carried out on *in-situ* SR-PXD data collected for **S3** and the Rietveld refinement on the SR-PXD data is seen in Fig. 1. The quartz capillary contributes significantly to the background at low 2θ values.

For all three samples, the observed Bragg reflections can be assigned to either the reactants, KAlH_4 or NH_3BH_3 , the reaction product, $\text{K}[\text{Al}(\text{NH}_2\text{BH}_3)_4]$, or the decomposition product, KBH_4 . The contrast between the presence of NH_3BH_3 in **S1** and KBH_4 in **S3** is further evident from TPPA in which the foaming of NH_3BH_3 is clearly observed in **S1** whereas only a minor volume change is observed for **S3** due to the gas release following decomposition (see Figs. S1 and S2).

Structural analysis

The Rietveld refined structure was optimized using DFT owing to multiple options for hydrogen positions. Three

Table 1 – Overview of sample compositions determined by Rietveld refinement of the SR-PXD data.

Sample	Compound				Milling time [h]
	K[Al(NH ₂ BH ₃) ₄] (wt%)	NH ₃ BH ₃ (wt%)	KAlH ₄ (wt%)	KBH ₄ (wt%)	
S1	67	21	12	0	8
S2	91	0.1	1.7	7.5	10
S3	67	3.6	3.1	26	12

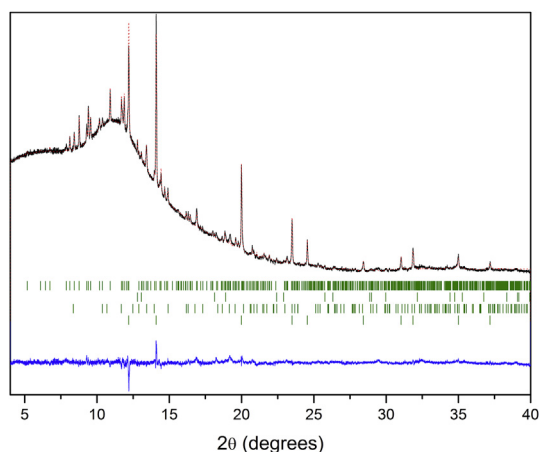


Fig. 1 – Rietveld refinement of the SR-PXD diffractogram of KAlH₄–NH₃BH₃ (1:4, S3, RT) containing K[Al(NH₂BH₃)₄] (upper green marker), NH₃BH₃ (second green marker), KAlH₄ (third green marker), and KBH₄ (lower green marker) ($\lambda = 0.8259$ Å). Observed data (Y_{obs} , red curve), Rietveld refinement profile (Y_{calc} , black curve), and difference plot ($Y_{\text{obs}} - Y_{\text{calc}}$, blue curve). Agreement factors, corrected for background, are $\chi^2 = 2.64$, $R_{\text{exp}} = 14.1\%$, $R_{\text{wp}} = 22.9\%$, and $R_p = 40.0\%$. (For interpretation of the references to colour in this figure legend, the reader is referred to the web version of this article.)

independent structures were obtained by DFT optimization procedures, which all can be assigned to $P-1$ symmetry, the main difference being the unit cell orientation and density (within 1.5%). Also the positions of the hydrogen atoms are different in these three structures. Normal mode analysis at the gamma point revealed no instabilities in these structures. The ground state energy was within 5 meV per formula unit (structure with the highest density was less stable by 20 meV). Considering the accuracy of the calculations, the obtained results do not allow the selection of one optimal structure, thus the Rietveld refinement of calculated models was decisive in the selection of a model.

The new compound, K[Al(NH₂BH₃)₄], is isostructural to Na[Al(NH₂BH₃)₄] [40]. Indeed, introduction of the larger potassium cation leads to an increased unit cell while the α -angle becomes smaller, see Table 2. The Al³⁺ ions are tetrahedrally coordinated to [NH₂BH₃][−] through the nitrogen lone pair, see Fig. 2a, with Al–N distances ranging from 1.838(9) Å to 1.909(9) Å (Al–N bond lengths of 1.90 Å to 1.91 Å are obtained from the DFT structural optimization). The K⁺ ion is

Table 2 – Comparison of crystallographic data for the isostructural compounds Na[Al(NH₂BH₃)₄] and K[Al(NH₂BH₃)₄], using data collected at $T = 100$ °C [40] and RT, respectively.

	Na[Al(NH ₂ BH ₃) ₄]	K[Al(NH ₂ BH ₃) ₄]
Space group	$P-1$	$P-1$
a (Å)	9.4352(2)	9.7151(3)
b (Å)	7.7198(1)	7.8221(3)
c (Å)	7.6252(1)	7.8750(3)
α (°)	97.211(1)	95.358(3)
β (°)	109.223(2)	109.944(3)
γ (°)	89.728(2)	89.629(3)
Z	2	2
V (Å ³)	518.86(2)	559.74(4)
ρ (g cm ^{−3}) (calc.)	1.070	1.101
ρ_m (H ₂) (wt%)	11.90	10.87
ρ_v (H ₂) (kg H ₂ L ^{−1})	119.81	111.02

octahedrally coordinated to [NH₂BH₃][−] through the BH₃ group in zig-zag 1D chains, see Fig. 2b and c. Four of the six [NH₂BH₃][−] units in the octahedron facilitate the bridging between K⁺ of the 1D chains, while all six [NH₂BH₃][−] bridge the K⁺ to an Al³⁺ to connect the 1D chains in a 3D network, see Fig. 2b.

Different from Na[Al(NH₂BH₃)₄], our model suggests alternating bridging of the K⁺ ions in the structure of K[Al(NH₂BH₃)₄], between corner-/corner-interactions and edge-/corner-interactions with the BH₃ group and results in two different K–K distances of 4.314(6) Å and 5.030(6) Å. The K–B distances range from 3.131(8) Å to 3.602(9) Å (3.17 Å to 3.59 Å from DFT) comparable to the K–B distance in KBH₄ of approximately 3.36 Å [58]. Furthermore, N–H^{δ+}...^{δ−}H–B distances as short as 1.969(9) Å (1.95 Å from DFT) indicate that the structure is partially stabilized by dihydrogen bonds.

In-situ synchrotron radiation powder X-ray diffraction

In-situ SR-PXD data of KAlH₄–NH₃BH₃ (1:4, S3) are presented in Fig. 3. Initially, diffraction from the new compound K[Al(NH₂BH₃)₄], the reactants KAlH₄ and NH₃BH₃, and the decomposition product, KBH₄, are present. Only the most intense Bragg reflection from NH₃BH₃ is visible in the data and it disappears at $T = 75$ °C, which is low compared to the reported decomposition temperature at 110–120 °C [25,59]. However, no change in the diffracted intensity of the other compounds is observed, hence no reaction appears to occur. The diffracted intensity of K[Al(NH₂BH₃)₄] is reduced at $T = 95$ °C and disappears completely at $T = 105$ °C, apparently in a single-step decomposition reaction, which does not produce crystalline products. In this case, there is no observable change in intensity of KBH₄ after decomposition of K[Al(NH₂BH₃)₄], though at $T > 115$ °C there is a significant, almost threefold, increase in the full width at half maximum (FWHM) from 0.0738° at $T = 115$ °C to 0.2008° at $T = 170$ °C, which may be due to a reduction in particle size. However, in-situ SR-PXD data of KAlH₄–NH₃BH₃ (1:4, S1) ball milled for only 8 h, shown in Fig. S3, clearly show an increase in diffracted intensity of KBH₄ after decomposition of K[Al(NH₂BH₃)₄]. Weak Bragg reflections from KAlH₄ are observed during the

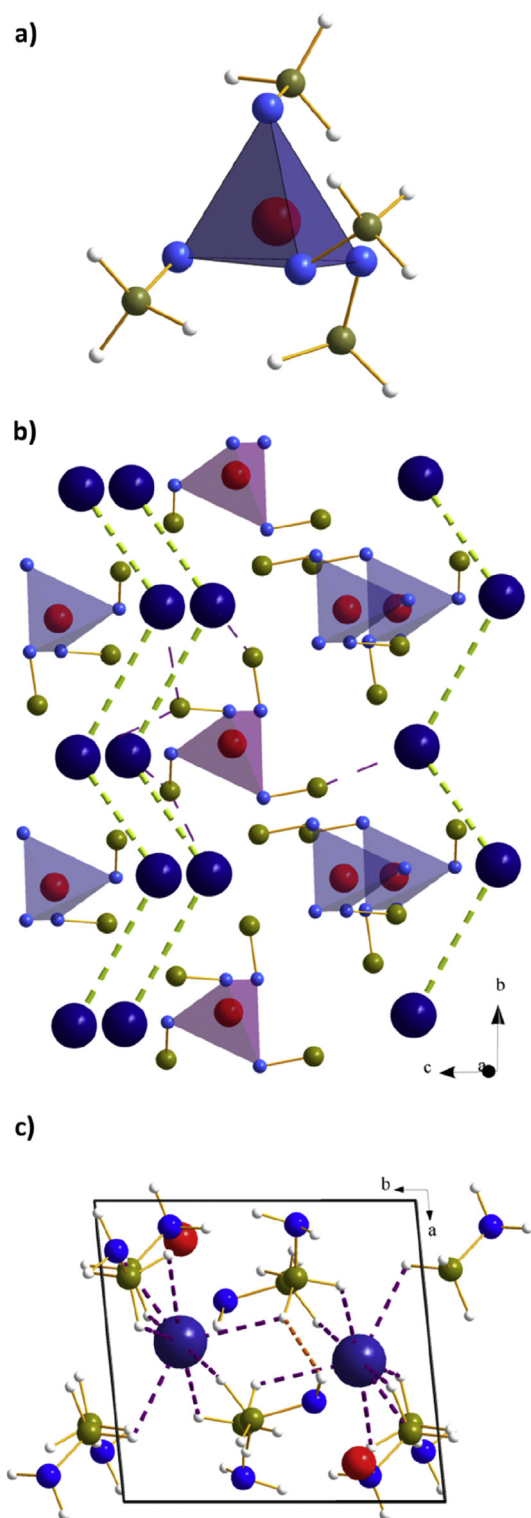


Fig. 2 – The crystal structure of $K[Al(NH_2BH_3)_4]$. (a) Coordination of the $[Al(NH_2BH_3)_4]^-$ complex. Color scheme: K, dark blue; Al, red; N, light blue; B, dark yellow. (b) The K^+ ions are organized as chains in the structure, illustrated as green dashed lines) and the linkage between these chains through the $[Al(NH_2BH_3)_4]^-$ complex (purple, dotted line). For simplicity, this is only shown in one case and hydrogen atoms have been omitted. Hence, the three chains shown are connected by the $[Al(NH_2BH_3)_4]^-$ complexes marked as

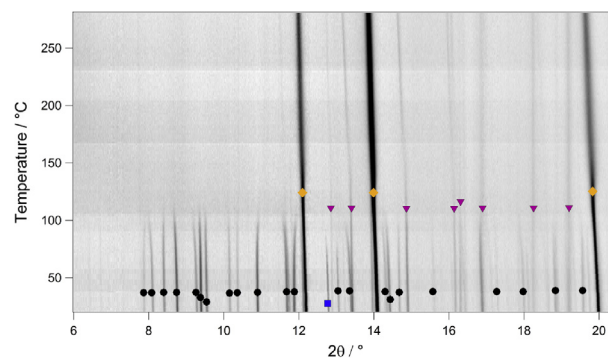


Fig. 3 – *In-situ* SR-PXD data of $KAlH_4-NH_3BH_3$ (1:4, S3) measured in the temperature range RT to 270 °C ($\Delta T/\Delta t = 6^\circ C \text{ min}^{-1}$, $\lambda = 0.8259 \text{ \AA}$). Symbols: $K[Al(NH_2BH_3)_4]$ black circle; NH_3BH_3 blue square; $KAlH_4$ purple triangle; KBH_4 orange diamonds. (For interpretation of the references to colour in this figure legend, the reader is referred to the web version of this article.)

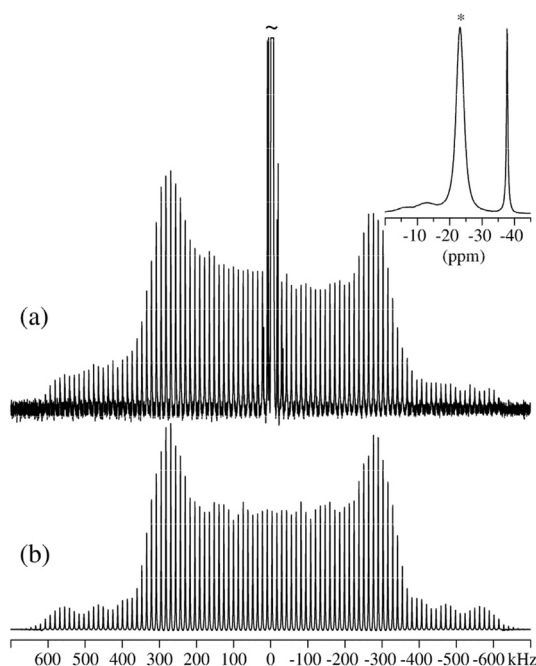


Fig. 4 – (a) ^{11}B MAS NMR spectrum (14.1 T) of the central and satellite transitions for $K[Al(NH_2BH_3)_4]$ (sample S2), obtained with a spinning frequency of $\nu_R = 13.0 \text{ kHz}$ and a 4-s relaxation delay. The inset illustrates the resonances from the central transitions. (b) Optimized simulation of the ssbs from the satellite transitions in (a), employing the ^{11}B parameters in Table 3 and a deviation from the magic angle of $\Delta\Theta = 0.0365^\circ$.

light red tetrahedra. (c) The unit cell of $K[Al(NH_2BH_3)_4]$ highlighting the coordination between K^+ and the BH_3 group via edge and corner interactions of hydrogen (purple, dotted lines). Additionally, a di-hydrogen bond is emphasized (orange, dotted line). (For interpretation of the references to colour in this figure legend, the reader is referred to the web version of this article.)

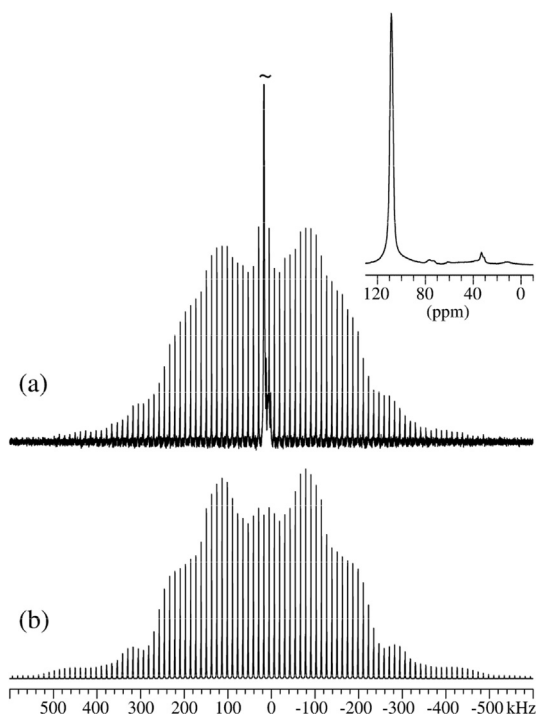


Fig. 5 – (a) ^{27}Al MAS NMR spectrum (14.1 T) of the central and satellite transitions for $\text{K}[\text{Al}(\text{NH}_2\text{BH}_3)_4]$ (sample S2), obtained with a spinning frequency of $\nu_R = 12.0$ kHz and a 4-s relaxation delay. The inset illustrates the spectra region for the central transitions. (b) Optimized simulation of the ssbs from the satellite transitions in (a), corresponding to the ^{27}Al parameters in Table 3.

entire *in-situ* SR-PXD experiment as decomposition does not occur before $T > 300$ °C [14].

^{11}B and ^{27}Al MAS NMR

^{11}B and ^{27}Al MAS NMR spectra of the central and satellite transitions for $\text{K}[\text{Al}(\text{NH}_2\text{BH}_3)_4]$ (sample S2) are shown in Figs. 4 and 5, respectively. The ^{11}B MAS NMR spectrum is dominated by the central transition at -22.3 ppm, and the associated spinning sidebands (ssbs) from the satellite transitions, which is assigned to the ^{11}B sites in the $\text{K}[\text{Al}(\text{NH}_2\text{BH}_3)_4]$ structure. This ^{11}B chemical shift is in agreement with a recent solution-state ^{11}B NMR study of $\text{K}[\text{Al}(\text{NH}_2\text{BH}_3)_4]$ [60]. In addition, minor centerband resonances at -6.3 ppm, -12.9 ppm, and -37.8 ppm are observed. The latter peak originates from KBH_4 , according to the ^{11}B chemical shift of -37.8 ± 0.2 ppm reported for this compound [61], which constitutes 9.9% of the ^{11}B intensity in the spectrum. The peaks with lower intensity at -6.3 ppm and -12.9 ppm can be assigned to $[\text{N}_3\text{BH}]$ and $[\text{N}_2\text{BH}_2]$ species, respectively, according to a recent ^{11}B MAS NMR study of lithium and potassium amidoboranes [42].

Least-squares optimization of simulated to experimental ssb intensities for the ^{11}B satellite transitions results in the ^{11}B isotropic chemical shift and quadrupole coupling parameters listed in Table 3 and the optimized simulation shown in Fig. 4b. The δ_{iso} and C_Q values for ^{11}B in $\text{K}[\text{Al}(\text{NH}_2\text{BH}_3)_4]$ are very similar to those reported for the two ammonia borane sites in

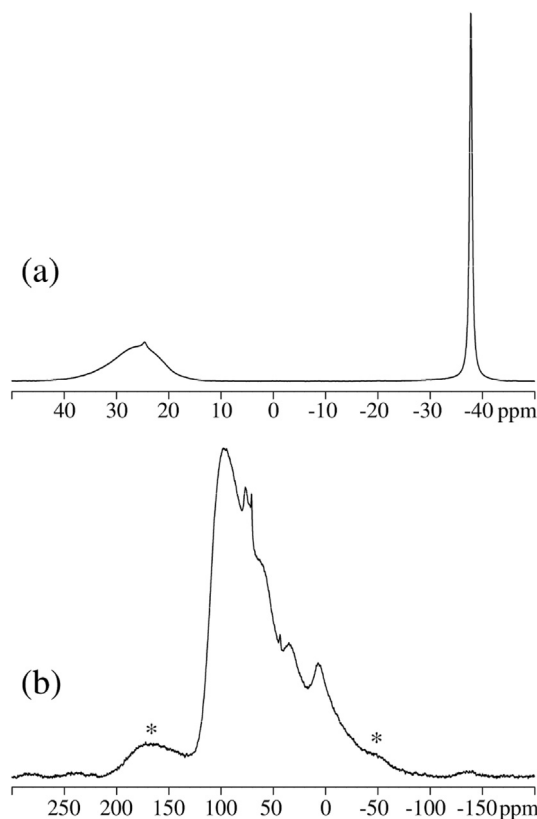


Fig. 6 – (a) ^{11}B and (b) ^{27}Al MAS NMR spectra (14.1 T) showing the central transition region for the decomposed sample of $\text{K}[\text{Al}(\text{NH}_2\text{BH}_3)_4]$. The ^{11}B spectrum is acquired with a spinning speed of $\nu_R = 12.0$ kHz and a relaxation delay of 30 s, whereas the ^{27}Al NMR spectrum, employed $\nu_R = 13.0$ kHz and a 4-s relaxation delay. Asterisks indicate spinning sidebands.

$\text{Mg}(\text{BH}_4)_2(\text{NH}_3\text{BH}_3)_2$ [35], where the isotropic chemical shift reflects the tetrahedral coordination of boron to three H^- and one N atom. However, only a single centerband resonance and ssb manifold are observed, despite the crystal structure

Table 3 – Experimental and calculated ^{11}B and ^{27}Al isotropic chemical shifts (δ_{iso}) and quadrupole coupling parameters (C_Q , η_Q) for $\text{K}[\text{Al}(\text{NH}_2\text{BH}_3)_4]$.^a

	δ_{iso} (ppm)	C_Q (MHz) ^b	η_Q ^c
^{11}B	-22.3 ± 0.2	1.26 ± 0.04	0.12 ± 0.02
B1	(-22.9)	(1.41)	(0.12)
B2	(-22.7)	(1.51)	(0.07)
B3	(-22.0)	(1.56)	(0.12)
B4	(-23.6)	(1.48)	(0.21)
^{27}Al	109.6 ± 0.3	2.41 ± 0.04	0.41 ± 0.02
	(110.7)	(1.83)	(0.21)

^a The numbers in brackets are calculated values from DFT calculations of the optimized structure.

^b Quadrupole coupling constant, $C_Q = eQV_{zz}/h$, where e is the charge of the electron, Q the nuclear quadrupole moment, h Planck's constant, and V_{zz} the principal element of the electric-field gradient tensor at the nuclear site, $|V_{zz}| \geq |V_{xx}| \geq |V_{yy}|$.

^c Quadrupole asymmetry parameter, $\eta_Q = (V_{yy} - V_{xx})/V_{zz}$.

for $\text{K}[\text{Al}(\text{NH}_2\text{BH}_3)_4]$ contains four crystallographically distinct ^{11}B sites. The absence of four resolved sites in the ^{11}B MAS NMR spectrum (Fig. 4a) may reflect dynamics in the structure and/or nearly identical chemical environments of the four sites, as reflected in the very similar δ_{iso} , C_Q and η_Q values calculated by DFT for the four sites (Table 3). In this context, we note that the calculated ^{11}B chemical shifts vary by only 1.6 ppm and are very close to the experimental values and that this similarity also holds for the C_Q and η_Q parameters.

The ^{27}Al central transition from KAlH_4 should be observed at 106 ppm [62], however, a close inspection of the line shape for the 109 ppm resonance from $\text{K}[\text{Al}(\text{NH}_2\text{BH}_3)_4]$ gives no indications of such a peak, thereby showing that the amount of KAlH_4 in the S2 sample must be very small, if present at all, which is in good agreement with the Rietveld refinement (Table 1), see Fig. 5a. Least-squares fitting to the intensities of the manifold of ssb's gives the δ_{iso} , C_Q , and η_Q parameters for the unique Al site in $\text{K}[\text{Al}(\text{NH}_2\text{BH}_3)_4]$ along with the simulated spectrum in Fig. 5b, which convincingly reproduces the experimental manifold of ssb's from the satellite transitions. Furthermore, the DFT calculated isotropic chemical shift (Table 3) agrees very well the experimental value and the calculated C_Q and η_Q values are of the same magnitude as those determined experimentally.

The ^{11}B MAS NMR spectrum of the decomposed $\text{K}[\text{Al}(\text{NH}_2\text{BH}_3)_4]$ sample, Fig. 6a, reveals a broad resonance at 26 ppm in addition to the narrow resonance at -37.8 ppm from KBH_4 . The featureless character of the peak at 26 ppm indicates a less-ordered/amorphous phase with a local ^{11}B coordination sphere that differs significantly from those of four-fold boron in BH_4^- and $\text{N}_{4-x}\text{BH}_x$ borane units. Similar resonances have been observed at 22 and 24 ppm by

decomposition of ammonia borane (NH_3BH_3) and potassium amidoborane (KNH_2BH_3), respectively, at elevated temperature [42], and are ascribed to the presence of trigonal boron coordinated to N and H (i.e., BN_3 , N_2BH , and/or NBH_2 units). The chemical shift of 26 ppm is in accord with boron in trigonal coordination, thereby suggesting that BN_3 , N_2BH , and/or NBH_2 species are formed in addition to KBH_4 during decomposition of $\text{K}[\text{Al}(\text{NH}_2\text{BH}_3)_4]$. The presence of less-ordered phases in the decomposition product is also in agreement with the ^{27}Al MAS NMR spectrum, Fig. 6b, which includes a number of rather broad and featureless resonances at approx. 96, 76, 61, 34 and 7 ppm. The peaks at 96, 76, and 61 ppm are ascribed to tetrahedrally coordinated Al whereas the resonances at 34 and 7 ppm are in accord with five-fold and octahedrally coordinated Al, respectively. The narrowest peak with lowest intensity at 76 ppm may originate from an AlO_4 impurity, whereas the other major resonances are ascribed to Al coordinated to H and/or N.

Thermal analysis

Simultaneous thermogravimetric analysis (TGA), differential scanning calorimetry (DSC), and mass spectrometry (MS) were measured for $\text{KAlH}_4\text{-NH}_3\text{BH}_3$ (1:4, S3), see Fig. 7. The DSC data reveal two exothermic thermal events. The first has onset at $T \sim 92^\circ\text{C}$ and maximum at $T \sim 104^\circ\text{C}$ which is associated with a mass loss of 1.3 wt% and a release of hydrogen, identified by MS. The second event initiates at $T \sim 139^\circ\text{C}$, peaks at $T = 153^\circ\text{C}$ and is accompanied by a mass loss of 4.2 wt%, which is mainly assigned to hydrogen according to the MS data. The separation between the first and second event is not well defined and appears to be a smooth transition. Tiny amounts of NH_3 ,

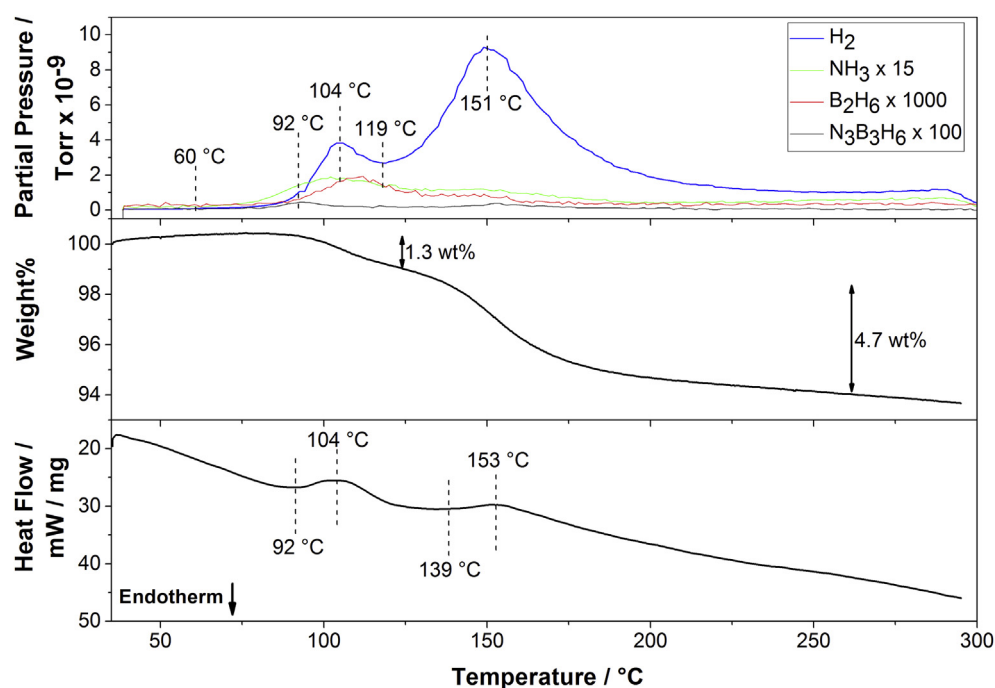


Fig. 7 – Differential scanning calorimetry (bottom), thermogravimetric analysis (middle), and mass spectrometry (top) data measured from RT to 300°C of $\text{KAlH}_4\text{-NH}_3\text{BH}_3$ (1:4, S3) ($\Delta T/\Delta t = 5^\circ\text{C}/\text{min}$, Ar flow).

$N_3B_3H_6$, and B_2H_6 (magnified 15, 100, and 1000 times, respectively, in Fig. 7) is also observed by MS in the two decomposition steps. MS data further reveal a minor H_2 , NH_3 , and $N_3B_3H_6$ release between $T \sim 60$ – 92 °C, which is not readily observed in TG-DSC. A total mass loss of 6.0 wt% is observed at ~ 262 °C.

Fourier-transformed infrared spectroscopy

From FT-IR (Fig. 8) of $KAlH_4-NH_3BH_3$ (1:4, S3) two bands from $N\cdots H$ stretching modes are observed between 3350 and 3250 cm^{-1} and three bands from $B\cdots H$ stretching modes between 2350 and 2200 cm^{-1} . These stretching modes are very similar to those observed for NH_3BH_3 . The $B\cdots H$ stretching modes probably have contributions from KBH_4 which were identified by PXD of the sample. However, the $Al\cdots H$ stretching mode observed in $KAlH_4$ at 1860 – 1460 cm^{-1} is no longer present, which is in agreement with the structure. Bands at 680 – 630 cm^{-1} are assigned to $Al\cdots N$ bending modes as reported for $Na[Al(NH_2BH_3)_4]$ [40]. Between 1600 – 1540 and 1100 – 1000 cm^{-1} $N\cdots H$ bending modes are present. Finally, $B\cdots H$ bending modes are located at 1380 and 1160 cm^{-1} . A calculated phonon spectrum (Fig. S4) is in good agreement with the FT-IR data, especially the $Al\cdots H$ stretching modes at 1860 – 1460 cm^{-1} are not present in the optimized $K[Al(NH_2BH_3)_4]$ structure.

Sieverts' measurement

The Sieverts' data in Fig. 9 reveal a slow gas release initiated at $T = 60$ °C which continues up to $T \sim 102$ °C where 0.3 wt% has been released. This supports the minor gas release observed by MS in a similar temperature range. At $T \sim 102$ °C, the first significant desorption step occurs, which releases an additional 1 wt% of gas between 102 and 128 °C. As observed in TGA-DSC, the second desorption step appears as a smooth transition from the first step and initiates at $T = 126$ °C. Further gas release of 4.2 wt% is observed in the second step. As the sample is kept at isothermal conditions at 200 °C, the total gas release amounts to ~ 6.0 wt%. These observations are in excellent agreement with the observations in TGA-DSC. A second desorption measurement was performed after hydrogenation of the sample.

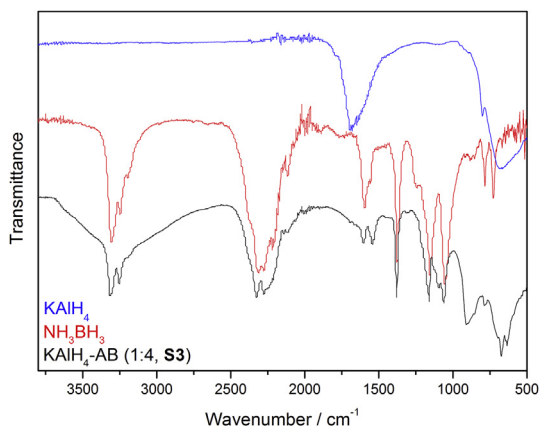


Fig. 8 – Comparison of the FT-IR spectra of $KAlH_4$, NH_3BH_3 , and $KAlH_4-NH_3BH_3$ (1:4, S3).

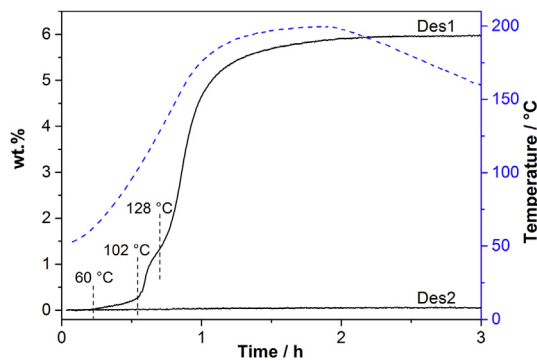


Fig. 9 – Sieverts' measurement of $KAlH_4-NH_3BH_3$ (1:4, S3) showing the two desorption experiments conducted in the temperature range RT to 200 °C ($\Delta T/\Delta t = 3$ °C/min, $p(H_2)_i = 10^{-3}$ bar).

However, the second measurement does not show any gas release, thus the sample did not absorb any hydrogen.

Discussion

The new potassium-containing aluminum-based amidoborane, $K[Al(NH_2BH_3)_4]$, differentiates from $Na[Al(NH_2BH_3)_4]$ in several ways. The structure contains two different $K^+\cdots K^+$ ion bridging modes as the structural model indicates corner/corner-interactions and edge/corner-interactions with the BH_3 group of the $NH_2BH_3^-$ ion due to the different K–K distances. From TG-DSC-MS data the decomposition of $K[Al(NH_2BH_3)_4]$ appears to occur in two exothermic steps, similar to the decomposition of $Na[Al(NH_2BH_3)_4]$, which is supported by Sieverts' measurement. However, a small gas release of 0.3 wt% is observed in the temperature range ~ 60 – 95 °C, which may be related to slow kinetics in the first decomposition step. The observed decomposition temperatures in TG-DSC-MS are 10–15 °C lower compared to the ones for $Na[Al(NH_2BH_3)_4]$ [40]. On the contrary, the SR-PXD data only suggest one decomposition step, which may be explained by a second decomposition step between two amorphous phases, which is not visible by X-ray diffraction, similar to observations made for $Na[Al(NH_2BH_3)_4]$. MS reveals a tiny amount of NH_3 , $N_3B_3H_6$, and B_2H_6 . However, based on the relative intensities, the NH_3 is suppressed compared to the Na-analogue and especially NH_3BH_3 . Finally, no hydrogen uptake is observed in the $K[Al(NH_2BH_3)_4]$ compound, which is contrary to $Na[Al(NH_2BH_3)_4]$ where hydrogen uptake was observed between the two amorphous phases at the same physical conditions as applied in this study. This suggests that the decomposition products of $K[Al(NH_2BH_3)_4]$ are more stable compared to those of $Na[Al(NH_2BH_3)_4]$, or that the decomposition is more exothermic, which is unfavorable. Further attempts to determine the decomposition products by PXD and FT-IR only support the formation of KBH_4 while a few Bragg reflections remain unassigned (see Fig. S5). Noticeably, the absence of Al Bragg reflections indicates that aluminum is chemically bound. This is supported by ^{27}Al MAS NMR which reveals the presence of four-, five-, and six-fold coordinated

aluminum in the decomposed sample. Finally, this may explain the suppression of the release of boron and nitrogen species, as they may be found in coordination with aluminum.

Conclusion

The crystal structure of $K[Al(NH_2BH_3)_4]$ was determined in a triclinic unit cell with space group symmetry $P\bar{1}$. The crystal structure contains $[K(NH_2BH_3)_6]^{5-}$ octahedra, which link the structure in a 3D network. The decomposition occurs in two distinct steps and the total release of hydrogen amounts to ~6 wt% H_2 . From ^{11}B and ^{27}Al MAS NMR and PXD, the decomposition mechanism has not been unambiguously determined due to its complexity. Hence, only KBH_4 can be identified as a decomposition product whereas aluminum is found in four-, five-, and six-fold coordination while boron is in three-fold coordination with nitrogen or hydrogen atoms as BN_3 , N_2BH , and/or NBH_2 units. A tiny amount of NH_3 , $N_3B_3H_6$, and B_2H_6 , is observed by MS in the two decomposition steps. However, the NH_3 release often observed in metal amidoboranes seem suppressed in this study. Finally, the decomposition is irreversible as Sieverts' data show no gas release after hydrogen absorption experiments at $p(H_2) = 130$ bar.

Acknowledgement

The work was supported by the Danish National Research Foundation, Center for Materials Crystallography (DNRF93), the Innovation Fund Denmark (HyFillFast), the Danish Research Council for Nature and Universe (Danscatt), the Carlsberg Foundation, and the Fonds de la Recherche Scientifique (FNRS). The authors would like to thank Diamond Light Source for access to beamline I11 and Annabelle Baker, Sarah Day, Claire Murray, and Stephen Thompson for assistance with data collection. Additionally, experiments were conducted at the BM01A beamline at the European Synchrotron Radiation Facility (ESRF), Grenoble, France. The authors are grateful to Dmitry Chernyshov and Iurii Dovgaliuk of the Swiss-Norwegian Beamlines for providing assistance in using beamline BM01A. Finally, support by the Polish National Science Center Project 2015/17/B/ST3/02478 and CPU allocation at the PL-Grid is kindly acknowledged.

Appendix A. Supplementary data

Supplementary data related to this article can be found at <https://doi.org/10.1016/j.ijhydene.2017.11.080>.

REFERENCES

- [1] Züttel A, Remhof A, Borgschulte A, Friedrichs O. Hydrogen: the future energy carrier. *Philos Trans Math Phys Eng Sci* 2010;368:3329–42. <https://doi.org/10.1098/rsta.2010.0113>.
- [2] Møller KT, Jensen TR, Akiba E, Li H. Hydrogen – a sustainable energy carrier. *Prog Nat Sci Mater Int* 2017;27:34–40. <https://doi.org/10.1016/j.pnsc.2016.12.014>.
- [3] Sakintuna B, Lamari-Darkrim F, Hirscher M. Metal hydride materials for solid hydrogen storage: a review. *Int J Hydrogen Energy* 2007;32:1121–40. <https://doi.org/10.1016/j.ijhydene.2006.11.022>.
- [4] Ould Amrouche S, Rekioua D, Rekioua T, Bacha S. Overview of energy storage in renewable energy systems. *Int J Hydrogen Energy* 2016;41:20914–27. <https://doi.org/10.1016/j.ijhydene.2016.06.243>.
- [5] Møller KT, Sheppard D, Ravnsbæk DB, Buckley CE, Akiba E, Li H-W, et al. Complex metal hydrides for hydrogen, thermal and electrochemical energy storage. *Energies* 2017;10:1645. <https://doi.org/10.3390/en10101645>.
- [6] Ley MB, Jepsen LH, Lee Y-S, Cho YW, Bellosta von Colbe JM, Dornheim M, et al. Complex hydrides for hydrogen storage – new perspectives. *Mater Today* 2014;17:122–8. <https://doi.org/10.1016/j.mattod.2014.02.013>.
- [7] Lai Q, Paskevicius M, Sheppard DA, Buckley CE, Thornton AW, Hill MR, et al. Hydrogen storage materials for mobile and stationary applications: current state of the art. *ChemSusChem* 2015;8:2789–825. <https://doi.org/10.1002/cssc.201500231>.
- [8] Durbin DJ, Malardier-Jugroot C. Review of hydrogen storage techniques for on board vehicle applications. *Int J Hydrogen Energy* 2013;38:14595–617. <https://doi.org/10.1016/j.ijhydene.2013.07.058>.
- [9] Klebanoff LE, Keller JO. 5 Years of hydrogen storage research in the U.S. DOE metal hydride center of excellence (MHCoe). *Int J Hydrogen Energy* 2013;38:4533–76. <https://doi.org/10.1016/j.ijhydene.2013.01.051>.
- [10] Callini E, Aguey-Zinsou K-F, Ahuja R, Ares JR, Bals S, Biliškov N, et al. Nanostructured materials for solid-state hydrogen storage: a review of the achievement of COST action MP1103. *Int J Hydrogen Energy* 2016;41:14404–28. <https://doi.org/10.1016/j.ijhydene.2016.04.025>.
- [11] Rusman NAA, Dahari M. A review on the current progress of metal hydrides material for solid-state hydrogen storage applications. *Int J Hydrogen Energy* 2016;41:12108–26. <https://doi.org/10.1016/j.ijhydene.2016.05.244>.
- [12] Bogdanović B, Schwickardi M. Ti-doped alkali metal aluminium hydrides as potential novel reversible hydrogen storage materials. *J Alloys Compd* 1997;253–254:1–9. [https://doi.org/10.1016/S0925-8388\(96\)03049-6](https://doi.org/10.1016/S0925-8388(96)03049-6).
- [13] Morioka H, Kakizaki K, Chung S-C, Yamada A. Reversible hydrogen decomposition of $KAlH_4$. *J Alloys Compd* 2003;353:310–4. [https://doi.org/10.1016/S0925-8388\(02\)01307-5](https://doi.org/10.1016/S0925-8388(02)01307-5).
- [14] Arnbjerg LM, Jensen TR. New compounds in the potassium-aluminium-hydrogen system observed during release and uptake of hydrogen. *Int J Hydrogen Energy* 2012;37:345–56. <https://doi.org/10.1016/j.ijhydene.2011.09.108>.
- [15] Ares JR, Aguey-Zinsou K-F, Leardini F, Ferrer JJ, Fernandez J-F, Guo Z-X, et al. Hydrogen absorption/desorption mechanism in potassium alanate ($KAlH_4$) and enhancement by $TiCl_3$ doping. *J Phys Chem C* 2009;113:6845–51. <https://doi.org/10.1021/jp807184v>.
- [16] Jepsen LH, Ley MB, Lee Y-S, Cho YW, Dornheim M, Jensen JO, et al. Boron–nitrogen based hydrides and reactive composites for hydrogen storage. *Mater Today* 2014;17:129–35. <https://doi.org/10.1016/j.mattod.2014.02.015>.
- [17] Hamilton CW, Baker RT, Staubitz A, Manners I. B–N compounds for chemical hydrogen storage. *Chem Soc Rev* 2009;38:279–93. <https://doi.org/10.1039/B800312M>.
- [18] Paskevicius M, Jepsen LH, Schouwink P, Černý R, Ravnsbæk DB, Filinchuk Y, et al. Metal borohydrides and derivatives – synthesis, structure and properties. *Chem Soc Rev* 2017;46:1565–634. <https://doi.org/10.1039/C6CS00705H>.
- [19] Callini E, Atakli ZÖK, Hauback BC, Orimo S, Jensen C, Dornheim M, et al. Complex and liquid hydrides for energy

- storage. *Appl Phys A* 2016;122:353. <https://doi.org/10.1007/s00339-016-9881-5>.
- [20] Staubitz A, Robertson APM, Manners I. Ammonia-borane and related compounds as dihydrogen sources. *Chem Rev* 2010;110:4079–124. <https://doi.org/10.1021/cr100088b>.
- [21] Stephens FH, Pons V, Baker RT. Ammonia–borane: the hydrogen source par excellence? *Dalton Trans* 2007:2613–26. <https://doi.org/10.1039/B703053C>.
- [22] Wang P. Solid-state thermolysis of ammonia borane and related materials for high-capacity hydrogen storage. *Dalton Trans* 2012;41:4296. <https://doi.org/10.1039/c2dt11778a>.
- [23] Demirci UB. Ammonia borane, a material with exceptional properties for chemical hydrogen storage. *Int J Hydrogen Energy* 2017;42:9978–10013. <https://doi.org/10.1016/j.ijhydene.2017.01.154>.
- [24] Wolf G, Baumann J, Baitalov F, Hoffmann FP. Calorimetric process monitoring of thermal decomposition of B–N–H compounds. *Thermochim Acta* 2000;343:19–25. [https://doi.org/10.1016/S0040-6031\(99\)00365-2](https://doi.org/10.1016/S0040-6031(99)00365-2).
- [25] Baitalov F, Baumann J, Wolf G, Jaenicke-Rößler K, Leitner G. Thermal decomposition of B–N–H compounds investigated by using combined thermoanalytical methods. *Thermochim Acta* 2002;391:159–68. [https://doi.org/10.1016/S0040-6031\(02\)00173-9](https://doi.org/10.1016/S0040-6031(02)00173-9).
- [26] Moussa G, Moury R, Demirci UB, Şener T, Miele P. Boron-based hydrides for chemical hydrogen storage. *Int J Energy Res* 2013;37:825–42. <https://doi.org/10.1002/er.3027>.
- [27] Chua YS, Chen P, Wu G, Xiong Z. Development of amidoboranes for hydrogen storage. *Chem Commun* 2011;47:5116–29. <https://doi.org/10.1039/C0CC05511E>.
- [28] Luedtke AT, Autrey T. Hydrogen release studies of alkali metal amidoboranes. *Inorg Chem* 2010;49:3905–10. <https://doi.org/10.1021/ic100119m>.
- [29] Xiong Z, Yong CK, Wu G, Chen P, Shaw W, Karkamkar A, et al. High-capacity hydrogen storage in lithium and sodium amidoboranes. *Nat Mater* 2008;7:138–41. <https://doi.org/10.1038/nmat2081>.
- [30] Diyabalanage HVK, Nakagawa T, Shrestha RP, Semelsberger TA, Davis BL, Scott BL, et al. Potassium(I) amidotrihydroborate: structure and hydrogen release. *J Am Chem Soc* 2010;132:11836–7. <https://doi.org/10.1021/ja100167z>.
- [31] Owarzany R, Leszczyński PJ, Fijalkowski KJ, Grochala W. Mono- and bimetallic amidoboranes. *Crystals* 2016;6:88. <https://doi.org/10.3390/cryst6080088>.
- [32] Tang Z, Zhang L, Wan L, Huang Z, Liu H, Guo Z, et al. Regeneration of alkaline metal amidoboranes with high purity. *Int J Hydrogen Energy* 2016;41:407–12. <https://doi.org/10.1016/j.ijhydene.2015.10.136>.
- [33] Wu H, Zhou W, Pinkerton FE, Meyer MS, Srinivas G, Yildirim T, et al. A new family of metal borohydride ammonia borane complexes: synthesis, structures, and hydrogen storage properties. *J Mater Chem* 2010;20:6550–6. <https://doi.org/10.1039/c0jm01542c>.
- [34] Luo J, Wu H, Zhou W, Kang X, Fang Z, Wang P. $\text{LiBH}_4 \cdot \text{NH}_3\text{BH}_3$: a new lithium borohydride ammonia borane compound with a novel structure and favorable hydrogen storage properties. *Int J Hydrogen Energy* 2012;37:10750–7. <https://doi.org/10.1016/j.ijhydene.2012.04.049>.
- [35] Jepsen LH, Ban V, Møller KT, Lee Y-S, Cho YW, Besenbacher F, et al. Synthesis, crystal structure, thermal decomposition, and ^{11}B MAS NMR characterization of $\text{Mg}(\text{BH}_4)_2 \cdot (\text{NH}_3\text{BH}_3)_2$. *J Phys Chem C* 2014;118:12141–53. <https://doi.org/10.1021/jp502788j>.
- [36] Chen X, Yuan F, Gu Q, Yu X. Synthesis, structures and hydrogen storage properties of two new H-enriched compounds: $\text{Mg}(\text{BH}_4)_2 \cdot (\text{NH}_3\text{BH}_3)_2$ and $\text{Mg}(\text{BH}_4)_2 \cdot (\text{NH}_3)_2 \cdot (\text{NH}_3\text{BH}_3)$. *Dalton Trans* 2013;42:14365–8. <https://doi.org/10.1039/C3DT52203B>.
- [37] Dovgaliuk I, Filinchuk Y. Aluminium complexes of B- and N-based hydrides: synthesis, structures and hydrogen storage properties. *Int J Hydrogen Energy* 2016;41:15489–504. <https://doi.org/10.1016/j.ijhydene.2016.05.196>.
- [38] Hawthorne MF, Jalisatgi SS, Safronov AV, Lee HB, Wu J. Chemical hydrogen storage using polyhedral borane anions and aluminum-ammonia-borane complexes. Columbia, MO: University of Missouri; 2010.
- [39] Dovgaliuk I, Le Duff CS, Robeyns K, Devillers M, Filinchuk Y. Mild dehydrogenation of ammonia borane complexed with aluminum borohydride. *Chem Mater* 2015;27:768–77. <https://doi.org/10.1021/cm503601h>.
- [40] Dovgaliuk I, Jepsen LH, Safin DA, Łodziana Z, Dyadkin V, Jensen TR, et al. A composite of complex and chemical hydrides yields the first Al-based amidoborane with improved hydrogen storage properties. *Chem Eur J* 2015;14:562–70. <https://doi.org/10.1002/chem.201501302>.
- [41] Nakagawa Y, Shinzato K, Nakagawa T, Nakajima K, Isobe S, Goshome K, et al. Synthesis, structural characterization, and hydrogen desorption properties of $\text{Na}[\text{Al}(\text{NH}_2\text{BH}_3)_4]$. *Int J Hydrogen Energy* 2017;42:6173–80. <https://doi.org/10.1016/j.ijhydene.2016.12.062>.
- [42] Shimoda K, Doi K, Nakagawa T, Zhang Y, Miyaoka H, Ichikawa T, et al. Comparative study of structural changes in NH_3BH_3 , LiNH_2BH_3 , and KNH_2BH_3 during dehydrogenation process. *J Phys Chem C* 2012;116:5957–64. <https://doi.org/10.1021/jp212351f>.
- [43] Hansen BRS, Møller KT, Paskevicius M, Dippel A-C, Walter P, Webb CJ, et al. In situ X-ray diffraction environments for high-pressure reactions. *J Appl Crystallogr* 2015;48:1234–41. <https://doi.org/10.1107/S1600576715011735>.
- [44] Favre-Nicolin V, Černý R. FOX, ‘free objects for crystallography’: a modular approach to *ab initio* structure determination from powder diffraction. *J Appl Crystallogr* 2002;35:734–43. <https://doi.org/10.1107/S0021889802015236>.
- [45] Rodríguez-Carvajal J. Recent advances in magnetic structure determination by neutron powder diffraction. *Phys B Condens Matter* 1993;192:55–69. [https://doi.org/10.1016/0921-4526\(93\)90108-I](https://doi.org/10.1016/0921-4526(93)90108-I).
- [46] Blöchl PE. Projector augmented-wave method. *Phys Rev B* 1994;50:17953–79. <https://doi.org/10.1103/PhysRevB.50.17953>.
- [47] Perdew JP, Burke K, Ernzerhof M. Generalized gradient approximation made simple. *Phys Rev Lett* 1996;77:3865–8. <https://doi.org/10.1103/PhysRevLett.77.3865>.
- [48] Grimme S, Antony J, Ehrlich S, Krieg H. A consistent and accurate *ab initio* parametrization of density functional dispersion correction (DFT-D) for the 94 elements H–Pu. *J Chem Phys* 2010;132:154104. <https://doi.org/10.1063/1.3382344>.
- [49] Kresse G, Furthmüller J. Efficient iterative schemes for *ab initio* total-energy calculations using a plane-wave basis set. *Phys Rev B* 1996;54:11169–86. <https://doi.org/10.1103/PhysRevB.54.11169>.
- [50] Pickard CJ, Mauri F. All-electron magnetic response with pseudopotentials: NMR chemical shifts. *Phys Rev B* 2001;63:245101. <https://doi.org/10.1103/PhysRevB.63.245101>.
- [51] Bonhomme C, Gervais C, Babonneau F, Coelho C, Pourpoint F, Azais T, et al. First-principles calculation of NMR parameters using the gauge including projector augmented wave method: a Chemist’s point of view. *Chem Rev* 2012;112:5733–79. <https://doi.org/10.1021/cr300108a>.
- [52] Hayashi S, Hayamizu K. Shift references in high-resolution solid-state NMR. *Bull Chem Soc Jpn* 1989;62:2429–30. <https://doi.org/10.1246/bcsj.62.2429>.

- [53] Jakobsen HJ, Skibsted J, Bildsøe H, Nielsen NC. Magic-angle spinning NMR spectra of satellite transitions for quadrupolar nuclei in solids. *J Magn Reson* 1969;1989(85):173–80. [https://doi.org/10.1016/0022-2364\(89\)90333-8](https://doi.org/10.1016/0022-2364(89)90333-8).
- [54] Łodziana Z, Błoński P, Yan Y, Rentsch D, Remhof A. NMR chemical shifts of ^{11}B in metal borohydrides from first-principle calculations. *J Phys Chem C* 2014;118:6594–603. <https://doi.org/10.1021/jp4120833>.
- [55] Lee Y-W, Clemens BM, Gross KJ. Novel Sieverts' type volumetric measurements of hydrogen storage properties for very small sample quantities. *J Alloys Compd* 2008;452:410–3. <https://doi.org/10.1016/j.jallcom.2006.11.014>.
- [56] Skibsted J, Nielsen NC, Bildsøe H, Jakobsen HJ. Satellite transitions in MAS NMR spectra of quadrupolar nuclei. *J Magn Reson* 1991;95:88–117. [https://doi.org/10.1016/0022-2364\(91\)90327-P](https://doi.org/10.1016/0022-2364(91)90327-P).
- [57] Paskevicius M, Ley MB, Sheppard DA, Jensen TR, Buckley CE. Eutectic melting in metal borohydrides. *Phys Chem Chem Phys* 2013;15:19774–89. <https://doi.org/10.1039/C3CP53920B>.
- [58] Luck RL, Schelter EJ. Potassium borohydride. *Acta Crystallogr C* 1999;55:IUC9900151. <https://doi.org/10.1107/S010827019909842X>.
- [59] Hu MG, Geanangel RA, Wendlandt WW. The thermal decomposition of ammonia borane. *Thermochim Acta* 1978;23:249–55. [https://doi.org/10.1016/0040-6031\(78\)85066-7](https://doi.org/10.1016/0040-6031(78)85066-7).
- [60] Chernysheva AM, Shelyganov PA, Kazakov IV, Timoshkin AY. Complex amidoboranes $\text{M}_2[\text{M}_1(\text{NH}_2\text{BH}_3)_4]$ ($\text{M}_1 = \text{Al, Ga}$; $\text{M}_2 = \text{Li, Na, K, Rb, Cs}$). *Russ J Gen Chem* 2017;87:665–9. <https://doi.org/10.1134/S1070363217040016>.
- [61] Ravnsbæk DB, Sørensen LH, Filinchuk Y, Reed D, Book D, Jakobsen HJ, et al. Mixed-anion and mixed-cation borohydride $\text{KZn}(\text{BH}_4)\text{Cl}_2$: synthesis, structure and thermal decomposition. *Eur J Inorg Chem* 2010;2010:1608–12. <https://doi.org/10.1002/ejic.201000119>.
- [62] Sorte EG, Emery SB, Majzoub EH, Ellis-Caleo T, Ma ZL, Hammann BA, et al. NMR study of anion dynamics in solid KAlH_4 . *J Phys Chem C* 2014;118:5725–32. <https://doi.org/10.1021/jp5001978>.